VISCOELASTIC PROPERTIES OF A PERFLUOROALKYLPOLYETHER LUBRICANT (MLO-71-6)

James F. Dill

Catholic University of America

Prepared for:

Office of Naval Research
Air Force Aero Propulsion Laboratory

January 1975

AD A006660

Security Classification 083166

DOCUMENT CONTROL DATA - R & D

(Security classification of title, body of abstract and indexing annotation must be entered when the overall report is classified)

1. ORIGINATING ACTIVITY (Corporate author)

Vitreous State Laboratory
TheCatholic University of America
Washington, DC 20064

2a. REPORT SECURITY CLASSIFICATION

UNCLASSIFIED

2b. GROUP

3. REPORT TITLE

Viscoelastic Properties of a Perfluoroalkylpolyether Lubricant (MLO-71-6)

4. DESCRIPTIVE NOTES (Type of report and inclusive dates)

Technical Report #3

5. AUTHOR(S) (First name, middle initial, last name)

James F. Dill

6. REPORT DATE

January, 1975

7a. TOTAL NO. OF PAGES

24

7b. NO. OF REFS

4

8a. CONTRACT OR GRANT NO.

NOOO14-67-A-0377-0018

b. PROJECT NO.

NR229-007

c. Funds supplied by Lubrication Branch, Fuels and Lubrication Division, AFAPL/SFL, WPAFT, Ohio under APAPL

d.

9a. ORIGINATOR'S REPORT NUMBER(S)

Technical Report #3

9b. OTHER REPORT NO(S) (Any other numbers that may be assigned this report)

10. DISTRIBUTION STATEMENT MIPR FY 14557400413

Reproduction in whole or in part is permitted for any purpose of the U.S. Govenment. Approved for Public Release: Distribution Unlimited.

11. SUPPLEMENTARY NOTES

12. SPONSORING MILITARY ACTIVITY

Office of Naval Research

13. ABSTRACT

Results of a study of the viscoelastic properties of a synthetic perfluoroalkylpolyether lubricant Krytox 143 AC (ML)-71-6) are described. Data were obtained using laser light scattering, ultrasonic and standard viscometric techniques. Viscosities of over 10^8 poise have been measured. Comparison is made with results reported on fluid of the same type by A. Cameron and G. Paul using their dynamic falling ball viscometer. It is shown that the observed differences between our results and that of Cameron and Paul cannot simply be interpreted in terms of differences between static and dynamic viscosities.

DD FORM 1 NOV 68 1473

Security Classification

VISCOELASTIC PROPERTIES OF A PERFLUOROALKYLPOLYETHER LUBRICANT (MLO -71-6)

TECHNICAL REPORT No. 3

N00014-67-A-0377-0018

by

J. Dill

Vitreous State Laboratory

The Catholic University of America

Washington, D.C. 20064

January, 1975

I INTRODUCTION

The purpose of this report is to present the results of a study of the pressure and temperature dependence of viscoelastic properties of the lubricant KRYTOX 143 AC(MLO-71-6) using light scattering and ultrasonic techniques. The techniques used included Brillouin scattering, digital correlation spectroscopy, low frequency ultrasonics as well as standard falling slug viscometry and capillary viscometry. The details of the techniques used have been previously described in detail in our technical reports Number 1 and Number 2 and therefore will not be presented again here in detail. Only those equations necessary for treatment of data will be included. Comparison of the results of this study with previous data in this fluid reported by Midwest Research for the bulk modulus and pressure dependence of the viscosity will be made. Comparison will also be made with reported data of Cameron and Paul where calculations of the viscosity were made using their optical falling ball viscometer. The sample of Krytox 143 AC was supplied by AFML at Wright-Patterson AFB and was known to be of the same type as that used by A. Cameron; as such we feel that for the first time the data presented here provide a detailed comparison of Cameron's technique with more conventional viscometric trchniques on samples known to be identical.

II Modulus Results

Measurements of the longitudinal modulus were made using both Brillouin scattering and low frequency ultrasonic techniques. Brillouin scattering measurements were made as a function of both temperature and pressure while the ultrasonic measurements were only made as a function of temperature.

A. Temperature Measurements

Measurements of the longitudinal Brillouin frequency shift were made at 1 atmosphere from -30 C to 220 C. From the measured values of the Brillouin shift frequency, ω_B, values for the longitudinal sound velocity were calculated using the relation

$$v_L = \frac{\lambda_o \omega_B}{\sqrt{2}\, n}$$

where λ_o is the wavelength of the incident light in vacuum and n is the index of refraction. Values of the longitudinal modulus are then calculated using the relation

$$M = \rho v_L^2$$

Calculations were performed using density data extrapolated from that reported in Midwest Research report AFML-TR-70-32, Part III and index of refraction values obtained from the density using the Eykman equation

$$\frac{n^2-1}{n+0.4} = K\rho \quad .$$

Constants for the Eykman equation were calculated from an initial value of n measured at 1 atmosphere and 22 C. Table I. contains the results of these measurements of the temperature dependence of the longitudinal modulus. Included are the values of the index of refraction and density used in the calculations. In the temperature range -30C to +30 C measured values correspond to the infinite frequency longitudinal modulus M_∞ and above 100 C they yielded the low frequency longitudinal or bulk modulus since the two are equal at low frequencies). In the temperature range +30 C to + 100 C measured values were in the relaxation region.

Temperature measurements of the longitudinal modulus were also made at 2 Mhz using ultrasonic "sing-around" techniques. These measurements gave values of the low frequency modulus from +60 C to + 133 C. Below 60 C this technique measured values in the relaxation region. At the lowest temperature (-60 C) the measured value was almost the infinite frequency value. These values are given in Table II. Results of both the temperature measurements of the longitudinal modulus are shown graphically in Fig. 1.

TABLE I: BRILLOUIN SCATTERING vs. TEMPERATURE

T(°C)	ω_B(Ghz)	n	V_L(m/sec)	ρ (gm/cm^3)	M(x10^{10}dynes/cm^2)
-30	4.96	1.316	1372	1.992	3.75
-20	4.75	1.313	1312	1.975	3.40
-10	4.47	1.310	1240	1.958	3.01
0	4.22	1.308	1175	1.941	2.68
10	3.93	1.305	1095	1.925	2.31
20	3.68	1.301	1030	1.909	2.03
40	3.23	1.296	906	1.875	1.54
60	2.79	1.291	787	1.842	1.14
80	2.35	1.285	665	1.809	0.80
100	2.04	1.279	581	1.777	0.60
120	1.88	1.273	536	1.742	0.50
140	1.69	1.266	485	1.701	0.40
160	1.59	1.262	457	1.677	0.35
180	1.50	1.256	434	1.643	0.31
200	1.38	1.249	403	1.601	0.26
220	1.28	1.245	374	1.577	0.22

TABLE II: LOW FREQUENCY ULTRASONIC RESULTS

T(°C)	V_L(m/sec)	ρ (gm/cm^3)	M(x10^{10} dynes/cm^2)
-60	1493	2.042	4.55
-50	1382	2.026	3.87
-40	1256	2.009	3.17
-30	1127	1.992	2.53
-20	973	1.975	1.87
-10	861	1.958	1.45
0	803	1.941	1.25
20	742	1.909	1.05
40	697	1.875	0.91
60	655	1.842	0.79
80	622	1.809	0.70
100	581	1.777	0.60
120	536	1.742	0.50
140	485	1.701	0.40

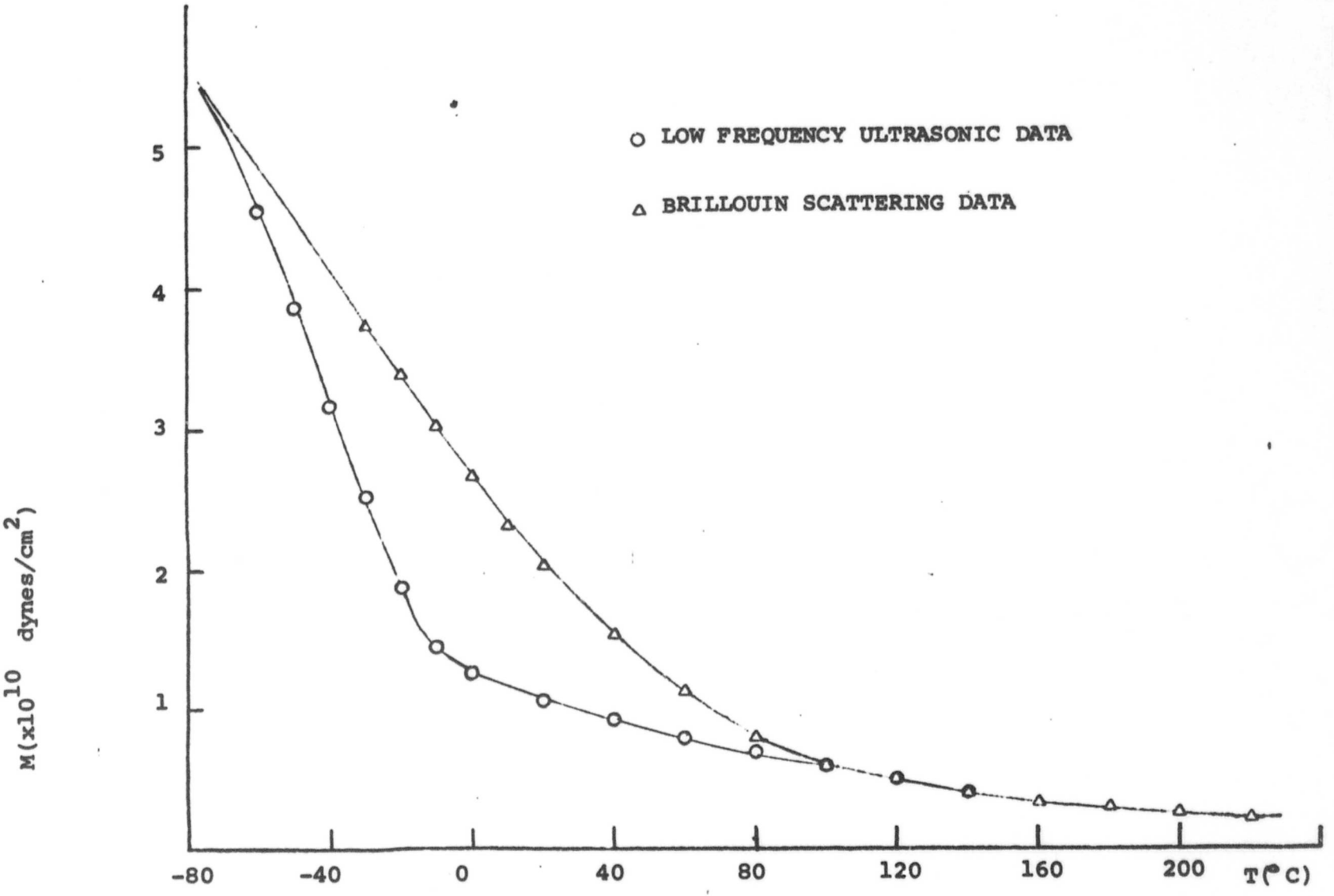

Fig. 1 Temperature Modulus Data

B. Pressure Measurements

Brillouin scattering measurements were performed as a function of pressure at 22.5 C from 1 atmosphere to 45,000 psi. These data as well as the corresponding densities and indices of refraction are given in Table III. Over the whole pressure range the measured values of the longitudinal modulus correspond to M_∞, the infinite frequency modulus. As can be seen in Fig. 2, the measured modulus was linear vs. pressure.

An interesting comparison can be made between the temperature and pressure modulus data when results are plotted vs. density. This comparison is shown in Fig. 3. From the correspondence of the results of the pressure and temperature measurements over a rather large range of overlap it seems that the temperature dependence of the longitudinal modulus is predominantly due to the temperature dependence of the density.

Also plotted in Fig. 3 are measurements of the isothermal bulk modulus reported by Midwest Research. Although the data measured here are adiabatic results, the difference between the adiabatic and isothermal moduli is usually small. As can be seen the MRI data agree with our results for the low frequency bulk modulus. Because of this agreement, the MRI data which were reported as a function of pressure have been used to obtain estimates of the bulk modulus where it is needed for calculation here.

C. Shear Modulus

Efforts have been made to measure the high frequency shear modulus over the whole temperature and pressure range of the longitudinal measurements, but Brillouin scattering from propagating shear waves was not observed. Our only conclusion as to the reasons for the failure of this portion of the experiment is that the optical coupling coefficient which determines the intensity of the light scattered by these particular fluctuations must be too small to cause a detectable amount of light to be scattered by their fluctuations. Because we were unable to directly measure G_∞, we have calculated the values used later from the measured M_∞ and K_o values using the relation

$$G_\infty = \frac{3}{8}(M_\infty - K_o)$$

where the assumption has been made that $\frac{4}{3}G_\infty = K_2$. Values of G_∞ calculated in this manner are also plotted in Fig. 2, and given in Table III along with the values of M_∞ used in the calculations.

TABLE III: PRESSURE MODULUS DATA

P(psi)	ω_B(Ghz)	n	V_L(m/sec)	ρ(gm/cm^3)	M_∞ (x10^{10}dynes/cm^2)	G_∞ (x10^{10}dynes/cm^2)
14.7	3.68	1.301	1030	1.909	2.03	.45
5000	4.38	1.310	1217	1.957	2.90	.72
10000	4.98	1.317	1376	1.995	3.78	.98
1500	5.51	1.323	1515	2.029	4.66	1.25
20000	5.99	1.322	1640	2.059	5.54	1.52
25000	6.43	1.332	1755	2.085	6.42	1.80
30000	6.83	1.336	1960	2.110	7.30	2.07
35000	7.21	1.341	1957	2.135	8.18	2.35
40000	7.58	1.345	2049	2.159	9.06	2.62
45000	7.92	1.349	2135	2.180	9.94	2.90

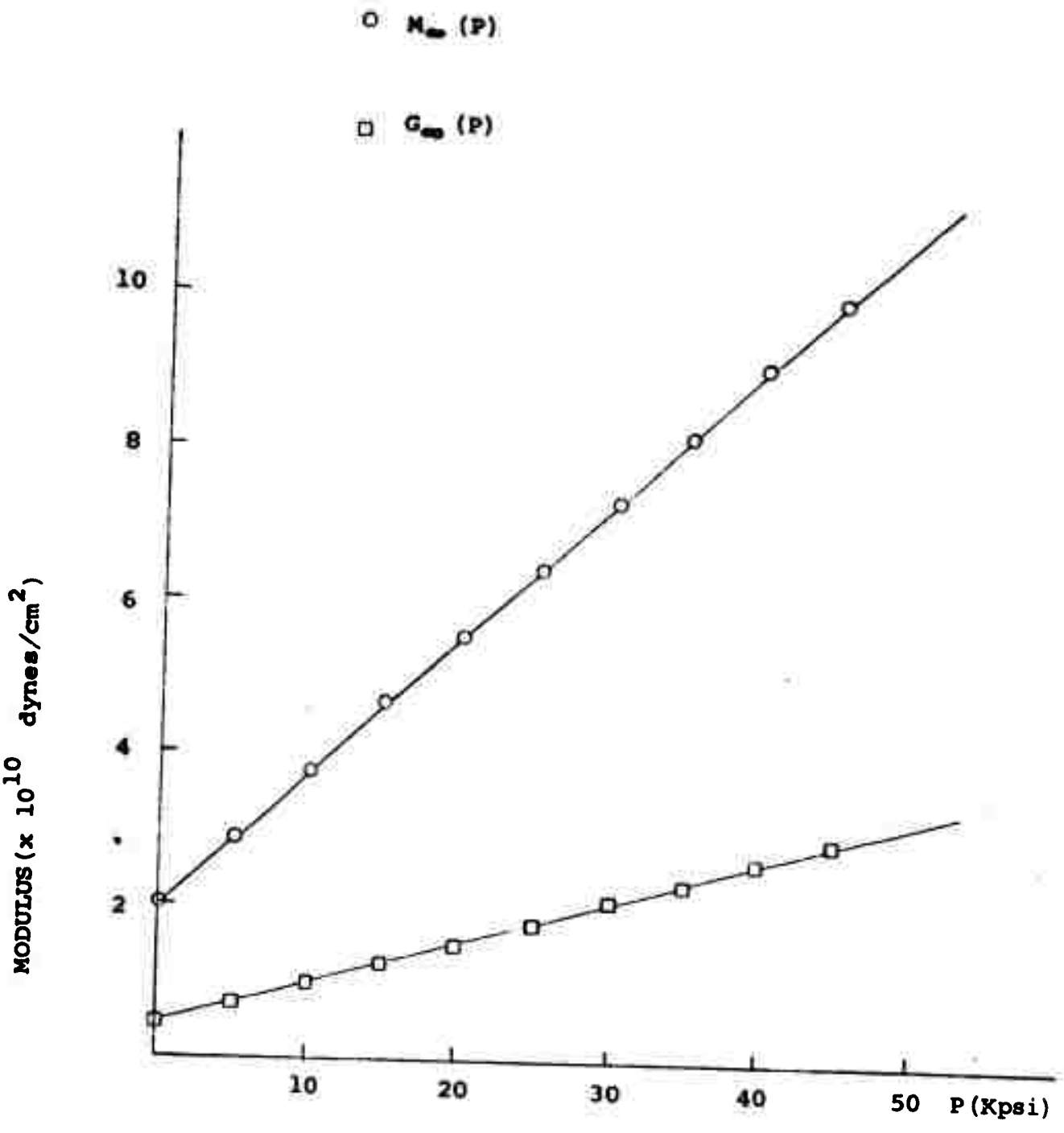

Fig. 2 Pressure Modulus Data

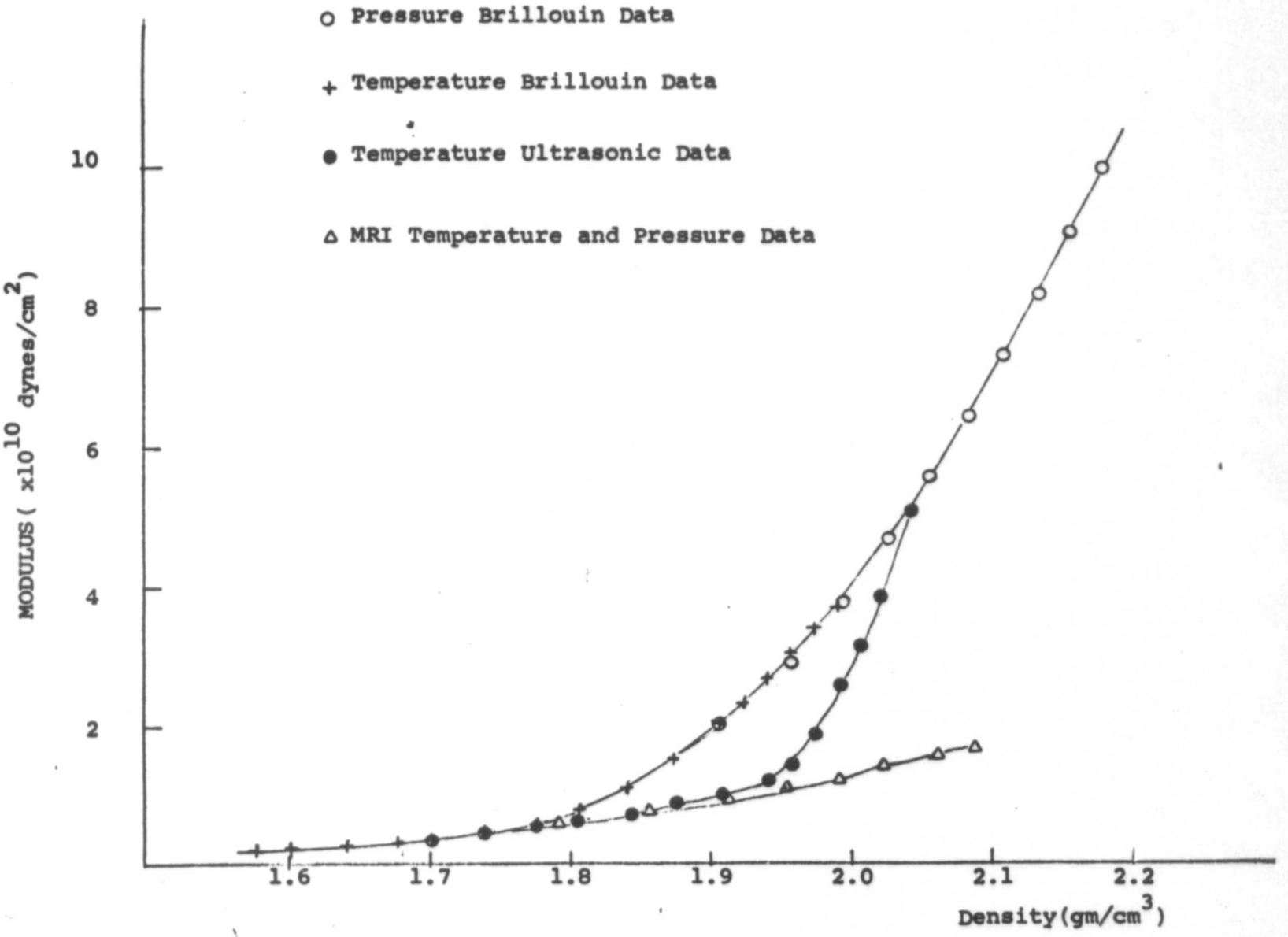

Fig. 3 Temperature and Pressure Modulus vs. Density

III Viscosity Measurements

Values of the shear viscosity were obtained using capillary, falling slug, and rotating spindle viscometers. Viscosity values were also calculated at high viscosities from the results of digital correlator light scattering measurements. Results were obtained as a function of both temperature and pressure using the different techniques depending on the region of measurement.

A. Temperature Measurements

Static viscosity measurements were made as a function of temperature from -65 C to 175 C. These values are presented in Table IV and are plotted in Fig. 4. The values measured here agree very well with those reported by Midwest Research in the temperature range of overlap, while the present measurements were taken to much higher viscosities than those previously reported. Both capillary viscometers and the rotating spindle viscometer were used to obtain the temperature results.

B. Pressure Measurements

Measurements of viscosity were made as a function of pressure at 20 C using a specially modified falling slug viscometer. The viscometer uses a LVDT (linear voltage differential transformer) to detect the motion of the slug, but the associated electronics have been modified to allow very small displacements (on the order of 20 microns) to be measured. Because of this modification, this system is capable of measuring viscosities to over 1×10^7 poise. The measurements described here have been carried out only to 3×10^5 poise because of difficulties with the pressure generating apparatus which have since been corrected. Values of the viscosity obtained in this manner are given in Table V and are plotted in Fig. 5.

Viscosities can also be calculated from digital correlator measurements of the structural relaxation function. Details of the results of these measurements will be presented in the next section. Only the results for the viscosities calculated in this manner will be reported here.

Values of G_∞ were calculated from measured values of M_∞ and K_o as described in Section II. The initial assumption was made that the average relaxation time associated with the measured correlation functions, $\langle\tau\rangle$, was equal to the shear relaxation time, τ_s. An effective longitudinal viscosity can be calculated in this manner using the relation

TABLE IV: TEMPERATURE VISCOSITY RESULTS

T(°C)	$1/T(\times 10^{3} K^{-1})$	η(Stokes)	$\rho(gm/cm^{3})$	η(Poise)	$\log_{10}\eta$(Poise)
-65	4.804	1.73×10^{8}	2.051	3.55×10^{8}	8.55
-60	4.692	1.74×10^{7}	2.042	3.55×10^{7}	7.55
-55	4.584	1.59×1^{6}	2.043	3.24×10^{6}	6.51
-50	4.481	2.47×10^{5}	2.026	5.01×10^{5}	5.70
-45	4.383	4.96×10^{4}	2.017	1×10^{5}	5.0
-40	4.289	1.57×10^{4}	2.009	3.16×10^{4}	4.50
-35	4.199	5.12×10^{3}	2.000	1.02×10^{4}	4.01
-30	4.113	2.00×10^{3}	1.992	3.98×10^{3}	3.60
-25	4.030	9.83×10^{2}	1.983	1.95×10^{3}	3.29
-20	3.950	4.73×10^{2}	1.975	9.33×10^{2}	2.97
-15	3.874	2.38×10^{2}	1.966	4.68×10^{2}	2.67
-10	3.800	1.28×10^{2}	1.958	2.51×10^{2}	2.40
0	3.661	4.49×10^{1}	1.941	8.71×10^{1}	1.94
10	3.532	1.80×10^{1}	1.925	3.47×10^{1}	1.54
20	3.411	8.30	1.909	1.58×10^{1}	1.20
30	3.299	4.40	1.892	8.32	.92
40	3.193	2.67	1.875	5.01	.70
50	3.095	1.63	1.858	3.02	.48
75	2.872	5.76×10^{-1}	1.818	1.05	.02
100	2.680	2.76×10^{-1}	1.777	4.90×10^{-1}	-.31
125	2.512	1.52×10^{-1}	1.734	2.63×10^{-1}	-.58
150	2.363	9.36×10^{-2}	1.693	1.58×10^{-1}	-.8
175	2.231	6.19×10^{-2}	1.652	1.02×10^{-1}	-.99

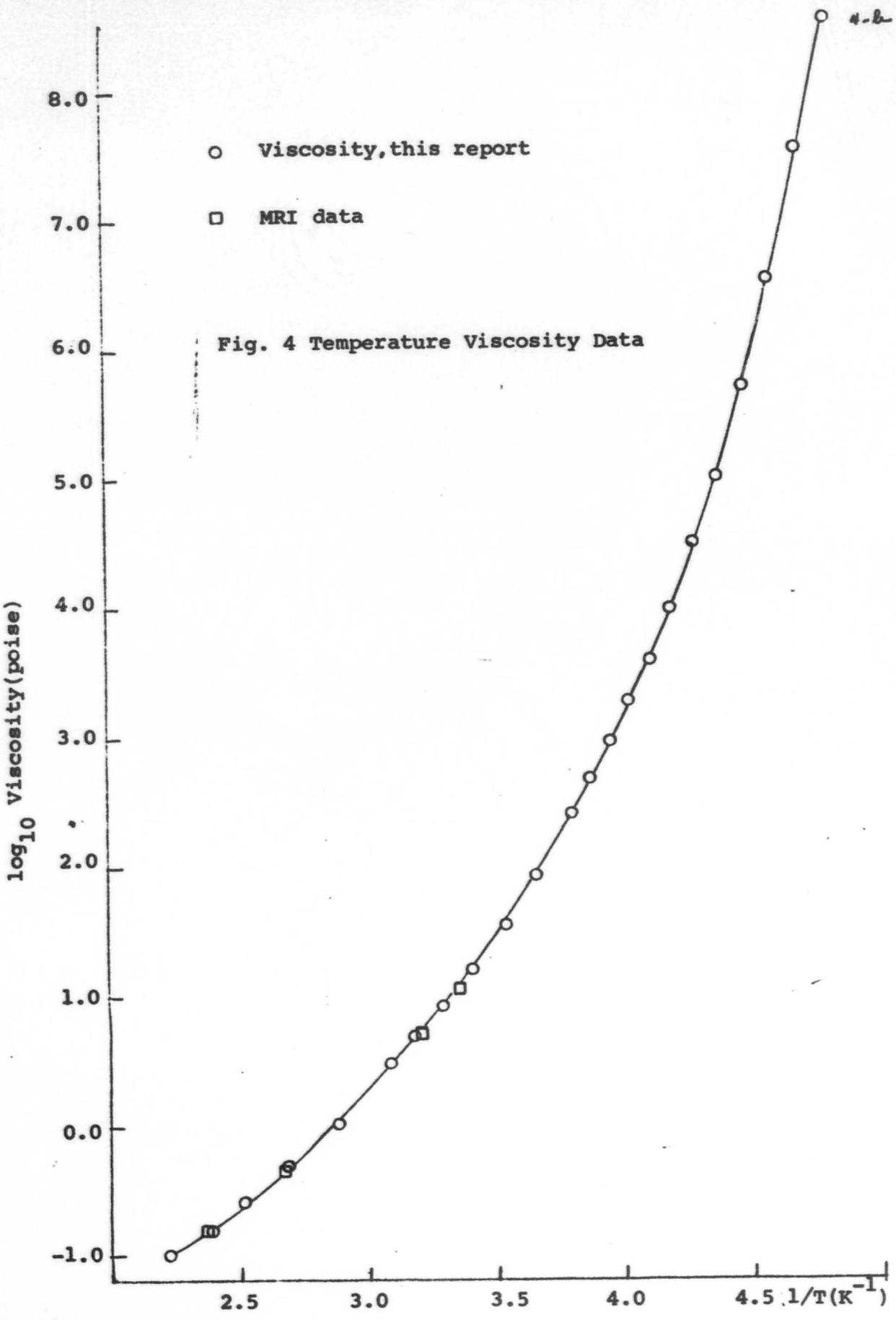

Fig. 4 Temperature Viscosity Data

TABLE V: PRESSURE VISCOMETER DATA (20°C)

P(psi)	η(Poise)	$\log_{10}$ η(Poise)
14.7	1.58×10^{1}	1.20
5000	8.91×10^{1}	1.95
10000	4.79×10^{2}	2.68
15000	2.45×10^{3}	3.39
20000	1.26×10^{4}	4.10
25000	6.31×10^{4}	4.81
30000	3.47×10^{5}	5.54

TABLE VI

P(psi)	$\langle\tau\rangle$(sec)	G_∞($\times 10^{10}$ dynes/cm^2)	η_L^{eff}(Poise)	η_s(Poise)
20000	5.23×10^{-5}	1.52	7.95×10^{5}	1.26×10^{4}
25000	2.26×10^{-4}	1.80	4.07×10^{6}	6.46×10^{4}
30000	1.01×10^{-3}	2.07	2.09×10^{7}	3.31×10^{5}
35000	4.56×10^{-3}	2.35	1.07×10^{8}	1.7×10^{6}
40000	2.07×10^{-2}	2.65	5.50×10^{8}	8.7×10^{6}
45000	9.72×10^{-2}	2.90	2.82×10^{9}	4.47×10^{7}
50000	4.56×10^{-1}	3.17	1.45×10^{10}	2.29×10^{8}

TABLE VII: DIGITAL CORRELATOR RESULTS

P(psi)	β	τ_o(sec)	exp ($1/4\beta^2$)	$\langle\tau\rangle$(sec)
20000	.4	1.10×10^{-5}	4.77	5.23×10^{-5}
25000	.37	3.64×10^{-5}	6.21	2.26×10^{-4}
30000	.34	1.16×10^{-4}	8.69	1.01×10^{-3}
35000	.31	3.38×10^{-4}	13.48	4.56×10^{-3}
40000	.28	8.55×10^{-4}	24.26	2.07×10^{-2}
45000	.26	2.41×10^{-3}	40.38	9.72×10^{-2}
50000	.24	5.94×10^{-3}	76.73	4.56×10^{-1}

$$\eta_L^{eff} = G_\infty \langle \tau \rangle$$

Values of η_L^{eff}, G_∞ and $\langle \tau \rangle$ are given in Table VI. These values reach over 1 x 10^{10} poise. For this effective viscosity to be equal to the shear viscosity, we must require that $\langle \tau \rangle = \tau_s$.

When comparison is made between the effective correlator viscosities and the shear viscosities measured by the falling slug viscometer (see Fig. 6), the data in the overlap pressure range from 20,000 psi to 30,000 psi shows that the ratio of $\langle \tau \rangle$ to τ_s is 63. The data obtained by the two techniques are clearly proportional as indicated by the parallel lines in Fig. 6. The correlator effective viscosities have been used to calculate the shear viscosity using the proportionality constant obtained from the overlap region. The shear viscosities obtained in this manner are also given in Table VI and are plotted in Fig. 5 as indicated. The viscosity measured at 20C is seen to follow a roughly exponential pressure dependence. Com ining the falling slug viscometer measurements with the correlator measurements of relaxation times has allowed the shear viscosity to be obtained to over 1 x 10^8 poise. Also shown in Fig. 5 are the pressure viscosity data reported by Midwest Research at higher temperatures. These data agree well with that taken in the present study at 20C.

C. Comparison with Cameron's Results

Fig. 7 is a plot of the viscosity data obtained in the present experiments and the data reported by Cameron and Paul in their Final Report AD 782231 on ONR Contract No. N00014-73-C-0107. The Cameron results are those taken at the longest measurement times and as such have been described by these authors as a measurement of the static shear viscosity. Since the samples used are of the same type, our data should have the same pressure viscosity behavior as that reported by Cameron and Paul. The data taken here were at 20 C. While the temperature is not reported in the Cameron report, in private communications the authors gave the temperature as being between 20 C and 25 C. As can be seen in Fig. 7, the actual shear viscosity data have none of the curvature seen in the Cameron data which falls first significantly below and then significantly above the measured shear viscosity. At the highest pressures (above the range of the present measurements) the Cameron data level off. There is no reason to expect such behavior from the data obtained in this study.

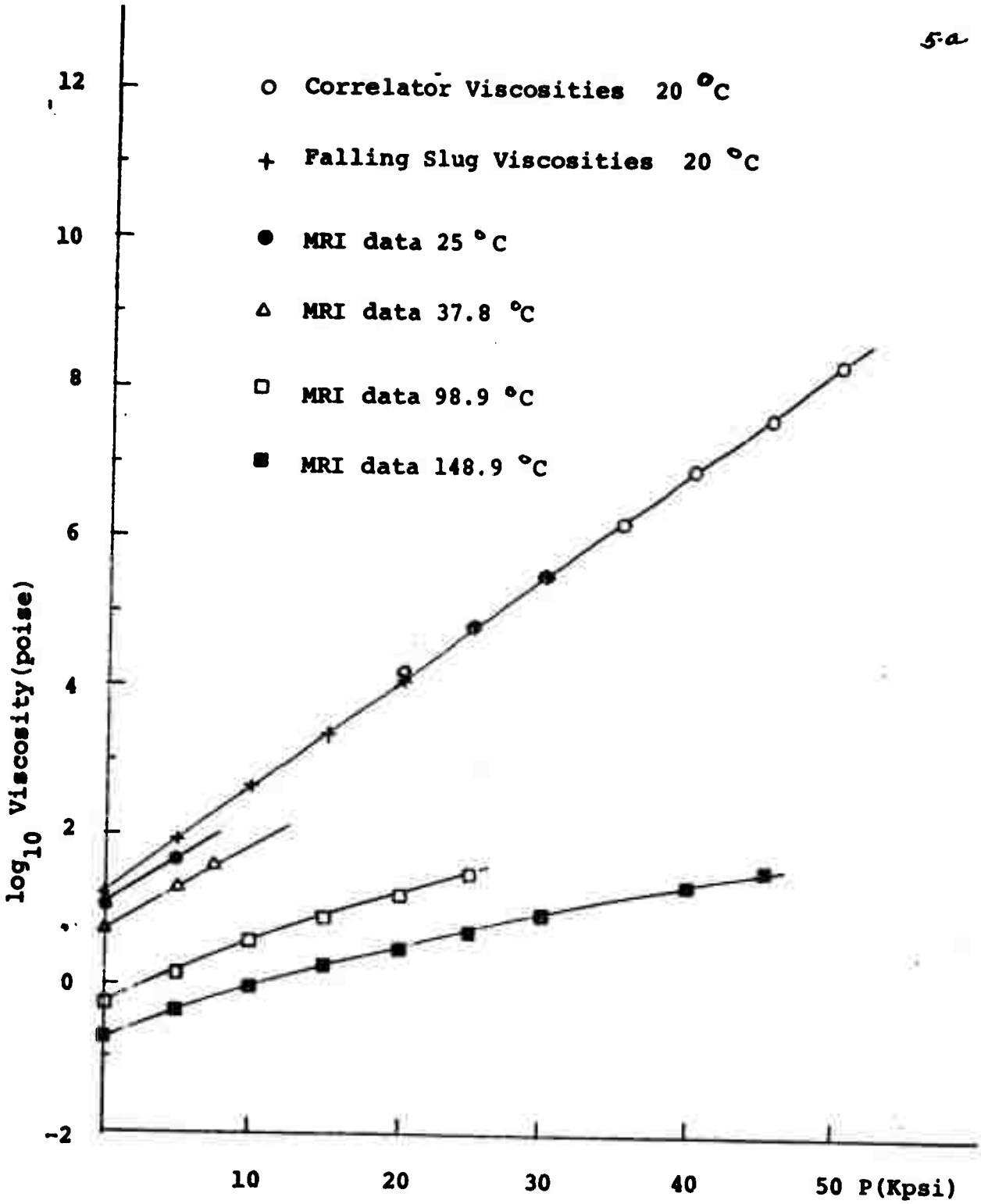

Fig. 5 Pressure Viscosity Data

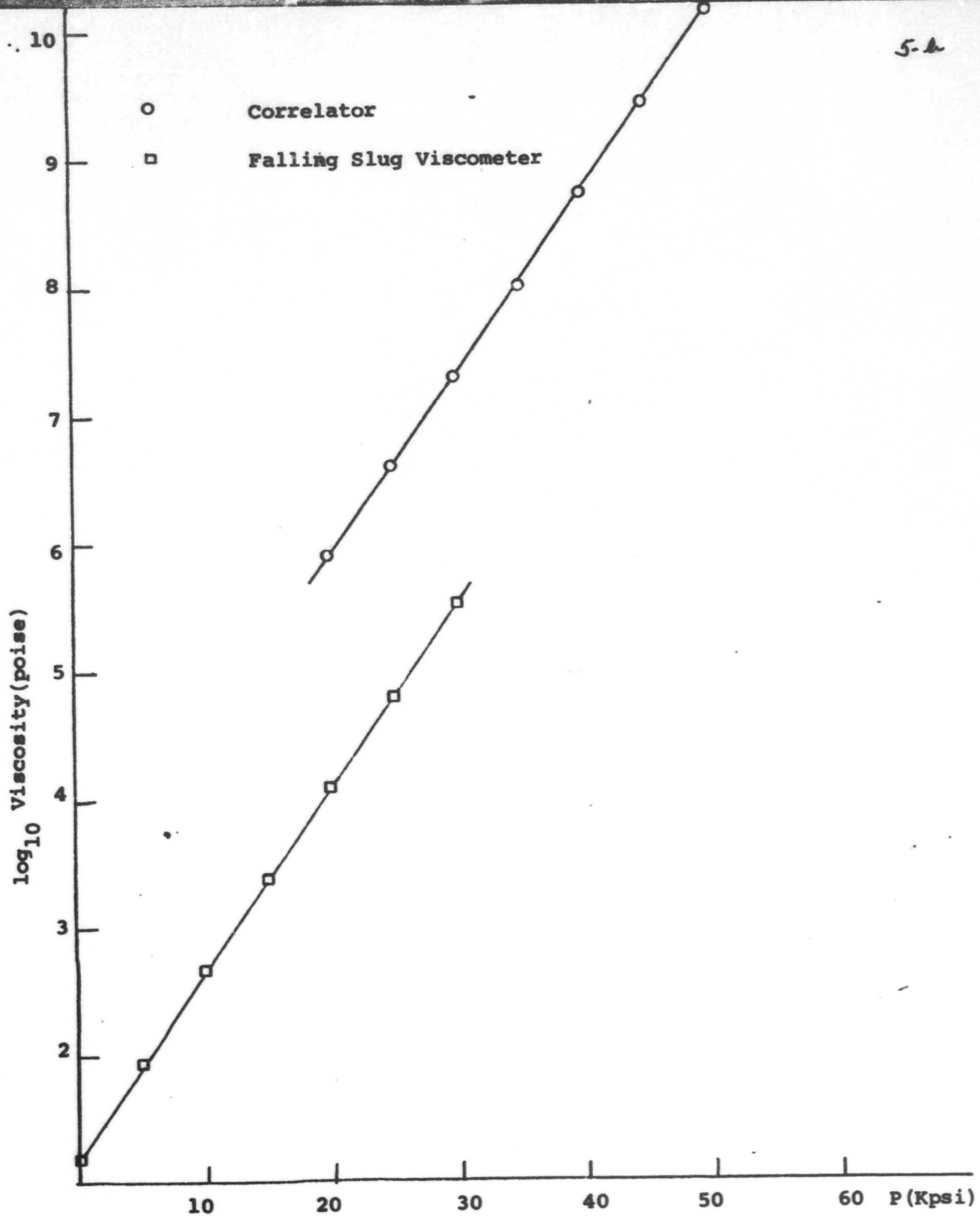

Fig. 6 Effective Correlator Viscosity and Shear Viscosity

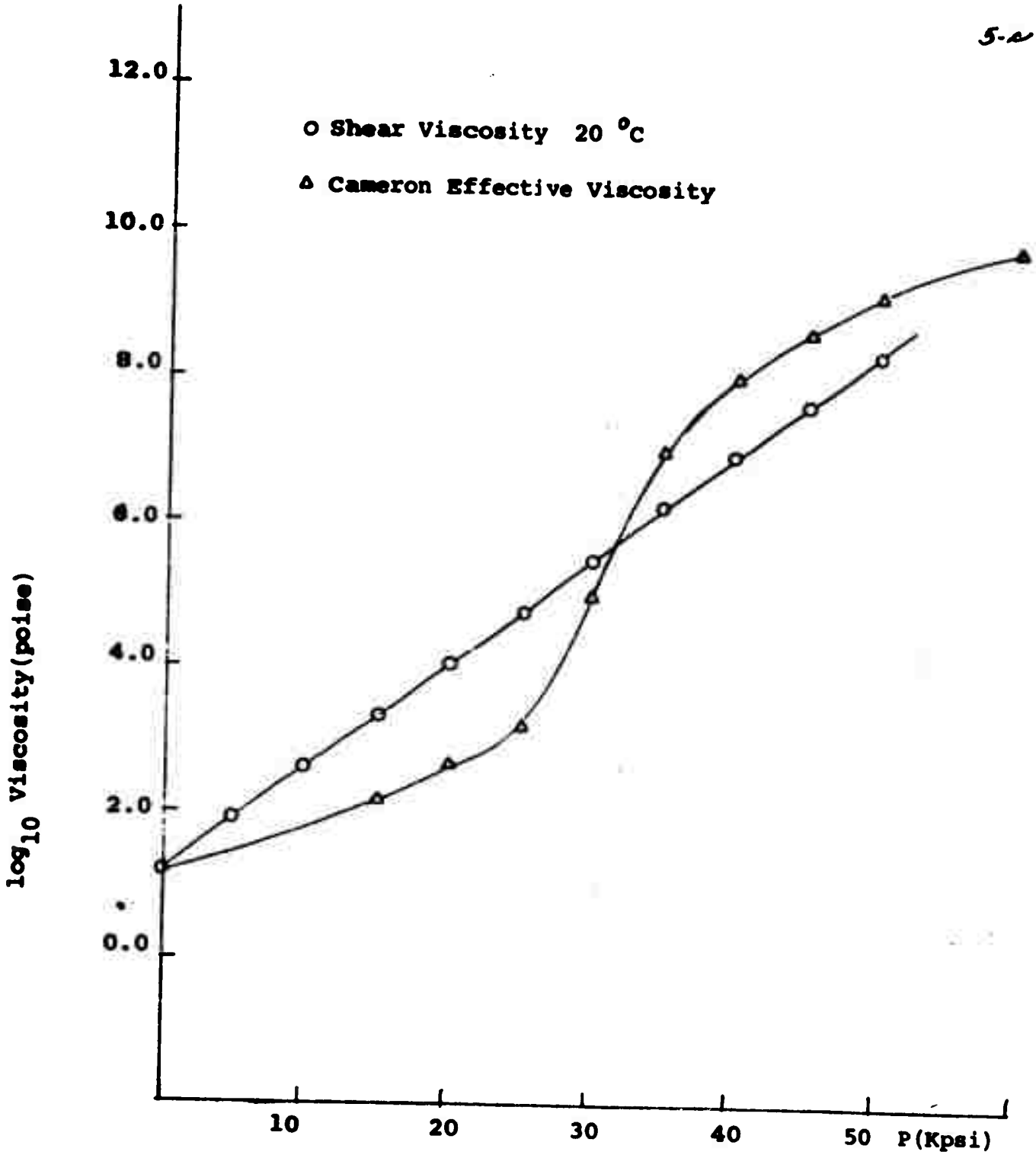

Fig.7 Comparison of Shear Viscosity and Cameron's Effective Viscosity

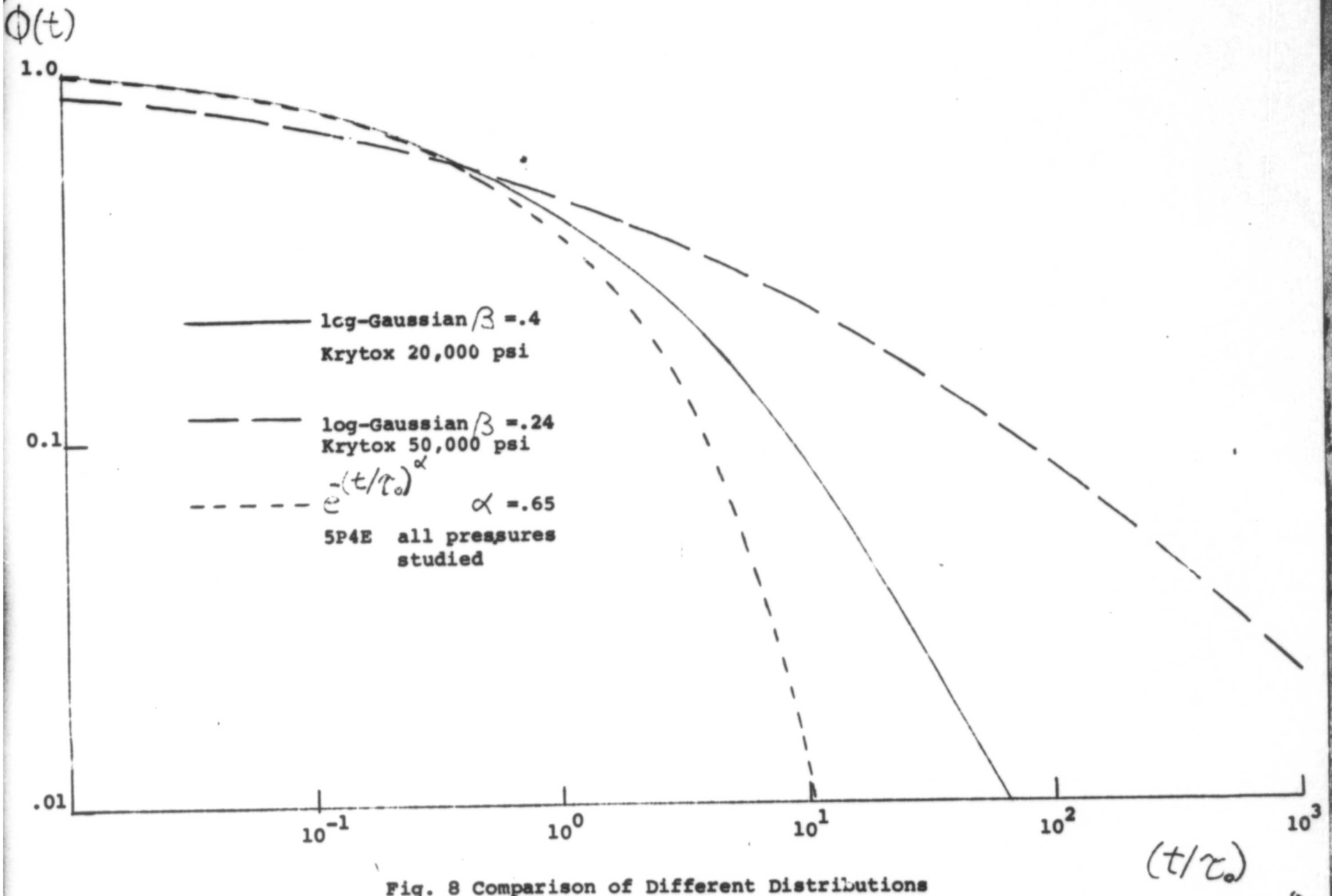

Fig. 8 Comparison of Different Distributions of Relaxation Times

In comparing our data with Cameron's results, we must ask what behavior we would expect of the differences between the experiments is due to the dynamic nature of Cameron's experiment. At low viscosities, i.e. low pressures, Cameron's data show no time dependent change in the calculated viscosity. In this region Cameron's calculated viscosity should be the equilibrium viscosity. Instead, the Cameron data fall at points almost two orders of magnitude below our viscosity data. At high viscosities where time dependent effects are observed (above 30,000 psi) if the difference is to be explained as a viscoelastic effect, where Cameron is measuring a dynamic viscosity rather than a static viscosity, viscoelastic theory would predict that the dynamic experiment should measure a viscosity which is less than the static viscosity. In this region, Cameron's data fall above the static viscosity data. Because of these differences, we feel that the differences between the two experiments cannot simply be explained in terms of expected differences between the static and dynamic viscosity.

IV Structural Relaxation Correlation Function Measurements

Measurements of the structural relaxation correlation function are reported here at 20 C over a pressure range from 20,000 to 50,000 psi. Over this range of study, the correlation function could not be described by a single distribution of relaxation times (as was seen in previous studies reported in our reports 1 and 2), but had to be fit by a distribution which changed in width as a function of pressure. It was found that the distribution which best fit the data over the whole pressure range was a log-Gaussian distribution. This distribution of relaxation times has the form

$$g(\tau) = e^{-[\beta \ln(\tau/\tau_o)]^2}$$

The form of the correlation function $\phi(t)$ was calculated for this distribution of relaxation times using the relation

$$\phi(t) = \int_0^\infty d\tau \; g(\tau) e^{-t/\tau}$$

by numerically performing the integration in the relation to give a numerical result for $\phi(t)$. The correlation functions calculated in this manner were then overlayed on the actual data to obtain a best fit at each pressure thus obtaining a value for β, the width of the distribution, and τ_o the position of the maximum in the distribution. The average relaxation time $\langle\tau\rangle$, which is needed for the calculation of the viscosity from measurements is calculated for the log-Gaussian distribution using the relation

$$\langle\tau\rangle = \tau_o e^{1/4\beta^2}$$

Values for β, τ_o and $\langle\tau\rangle$ are given in Table VII. Examples of the correlation functions which were used to fit the data at 20,000 psi and 50,000 psi are given in Fig. 8 to show how the shape changes over the range of measurement. The curves have been plotted on a reduced time scale $\log(\tau/\tau_o)$ for easy comparison. Because of the very broad nature of measured correlation functions in Krytox 143 AC obtaining the data was extremely time consuming since measurements had to be performed over a very large range of time scales to obtain data at any single pressure. Since the shape of the distribution was not constant as a function of pressure, the range of the correlator measurements were limited somewhat because the whole correlation function had to be obtained at each pressure. When the shape remains constant, measurements can be made where the whole correlation function is not obtained on the longest time scale, allowing relaxation times perhaps an order of magnitude or more longer than those reported here to be measured. Further study of the details of the correlation function in this fluid are presently being carried out. It is interesting to note, however, that the distributions obtained

here are considerably broader than those observed in measurements on other fluids which implies that viscoelastic effects may be of greater importance in Krytox 143 AC than in Fluids such as 5P4E which we have previously reported on. Also shown in Fig. 8 is the form of ϕ (t) for 5P4E which as can be seen is considerably narrower than even that at the lowest pressure in Krytox 143 AC.

REFERENCES

1. "Structural Relaxation by Digital-Correlation Spectroscopy," Technical Report No. 1, N00014-67-A-0377-0018.

2. "The Applicability of Light Scattering Spectroscopy to the Measurement of the Viscoelastic Parameters of Lubricants," Technical Report No. 2, N00014-67-A-0377-0018.

3. D. R. Wilson, Exploratory Development on Advanced Fluids and Lubricants in Extreme Environments by Mechanical Characterization Technical Report AFML-TR-70-32, Part III Jan. 1972.

4. A. Cameron, G. Paul, Final Report, ONR contract No. N00014-73-C-0107, AD 782231.